Novel Low Band Gap Small Molecule and Phenylenevinylene Copolymer with Cyanovinylene 4-Nitrophenyl Segments: Synthesis and Application for Efficient Bulk Heterojunction Solar Cells

ARTICLE *in* ACS APPLIED MATERIALS & INTERFACES · JANUARY 2010

Impact Factor: 6.72 · DOI: 10.1021/am9006897 · Source: PubMed

4 AUTHORS, INCLUDING:

John A Mikroyannidis
University of Patras
277 PUBLICATIONS **3,810** CITATIONS
SEE PROFILE

G. D. Sharma
The LNM Institute of Information Technolo…
231 PUBLICATIONS **2,729** CITATIONS
SEE PROFILE

ARTICLE

Novel Low Band Gap Small Molecule and Phenylenevinylene Copolymer with Cyanovinylene 4-Nitrophenyl Segments: Synthesis and Application for Efficient Bulk Heterojunction Solar Cells

John A. Mikroyannidis,*,† S. S. Sharma,‡ Y. K. Vijay,‡ and G. D. Sharma*,§,||

Chemical Technology Laboratory, Department of Chemistry, University of Patras, GR-26500 Patras, Greece, Physics Department, Molecular Electronic and Optoelectronic Device Laboratory, Jai Narain Vyas University, Jodhpur, Rajasthan 342005, India, Jaipur Engineering College, Kukas, Jaipur, Rajasthan, India, and Thin film & Membrane Science Laboratory, Department of Physics, University of Rajasthan, Jaipur, Rajasthan 302004, India

ABSTRACT A novel star-shaped small monomer **SM** containing a 1,3,5-triazine core and arms with terminal cyanovinylene 4-nitrophenyls was synthesized. Moreover, an alternating *p*-phenylenevinylene copolymer **P** containing thiophene with cyanovinylene 4-nitrophenyl side segments was synthesized by Heck coupling. Both **SM** and **P** showed broad absorption spectra with long-wavelength maximum at 630−648 nm, which for **P** is attributable to an intramolecular charge transfer. The optical band gap was 1.57 eV for **SM** and 1.70 eV for **P**. Both **SM** and **P** were blended with PCBM to study the donor−acceptor interactions on the blend film morphology and device characteristics of organic bulk heterojunction solar cells. A combination of characterization techniques including X-ray diffraction and optical topographical images were used to investigate the film morphology. The HOMO and LUMO levels of both **SM** and **P** are well-aligned with those of the PCBM acceptor, allowing efficient electron transfer and suitable open circuit voltage, leading to overall power conversion efficiencies (PCEs) of 2.53 and 1.43% for **SM**:PCBM and **P**:PCBM-based devices, respectively. The thermal annealing leads to suitable phase separation due to the increase in crystallinity of donor material and material distribution so that highly effective bulk heterojunction morphologies are obtained which further increases the PCE up to 3.82% and 2.37% for **SM**:PCBM and **P**:PCBM-based devices, respectively. These results are preliminary based on the illumination without using a solar simulator.

KEYWORDS: *p*-phenylnevinylene • small molecule solar cell • organic solar cells • triazine • bulk heterojunction solar cell • cyanovinylene.

INTRODUCTION

Organic solar cells generally use a blend of electron donor and acceptor materials in which nanoscale phase separation of the two components is created to achieve both quantitative charge generation after photoexcitation and effective collection of these charges. The most efficient bulk heterojunction (BHJ) solar cells of this type combine a conjugated polymer as an electron donor and a methanofullerene derivative as an electron acceptor. A fullerene derivative, [6,6]-phenyl-C_{61}-butyric acid methyl ester (PCBM), showing better solubility than C_{60} in common solvents, is a widely utilized acceptor. To further improve the performance, small band gap polymers have attracted considerable attention in recent years (1–16). The small band gap enhances the overlap of the polymer absorption spectrum with the solar emission that peaks around 700 nm (1.77 eV). The extended absorption potentially increases the photocurrent by absorbing more photons.

A successful and flexible strategy to design small band gap polymers involves the alternation of electron-rich and electron-deficient units along the polymer chain. In fact, varying the strength of the electron rich and electron deficient units allows judicious positioning of the energy levels of the polymer with respect to those of the acceptor. When designing small band gap polymers for photovoltaics, several aspects need to be taken into account. Decreasing the band gap can be achieved by either lowering the lowest unoccupied molecular orbital (LUMO) or raising the highest occupied molecular orbital (HOMO) of the polymer, or both. However, it is generally considered that a minimum offset of ∼0.3−0.4 eV between the LUMO of the donor and the LUMO of the acceptor is required to ensure quantitative charge separation at the donor/acceptor interface (17, 18).

Solution-processable small molecules have attractive features, such as lower band gap and higher charge carrier mobility than conjugated polymers. These small molecule donors, which can be more easily synthesized in various

* Corresponding author. Tel: +30 2610 997115(J.A.M.); 91-0291-2720857. Fax: +30 2610 997118 (J.A.M.); 91-0291-2720856 (G.D.S.). E-mail: mikroyan@chemistry.upatras.gr (J.A.M.); sharmagd_in@yahoo.com (G.D.S.).
Received for review October 10, 2009 and accepted December 6, 2009
† University of Patras.
‡ University of Rajasthan.
§ Jai Narain Vyas University.
|| Jaipur Engineering College, Kukas.
DOI: 10.1021/am9006897

Published on Web 12/16/2009

chemical structures and purified, are intrinsically more monodispersive and often environmentally more stable (16–18). There are several families of solution processable small molecules that have been used as donor materials in BHJ solar cells (19–22). Solution-processed small molecules that have been used for photovoltaic (PV) cells have been recently reviewed (23).

Dialkoxy-substituted poly(*p*-phenylene vinylene)s (PPVs), for example, poly[2-methoxy-5-(2′-ethyl-hexyloxy)-1,4-phenylene vinylene] (MEH-PPV) and poly[2-methoxy-5-(3′,7′-dimethyloctyloxy)-1,4-phenylene vinylene] (MDMO-PPV) show strong absorption in the visible light band (24–27). Notable power conversion efficiency (PCE) values of 2−3 % have been reproducibly achieved. Regioregular poly(3-hexylthiophene) (P3HT) is also a widely investigated polymer donor, from which repeatable PCE values of 3−5 % have been reported (24). Many optimization methods, such as using different solvents to fabricate the active layer, thermally annealing the active layer or the device, film forming speed, additives to the active layer, optical spacer, anode or cathode interfacial layer, and tandem structure, have been extensively carried out with P3HT, MEH-PPV, and MDMO-PPV as donors and have demonstrated significant improvements in the PV performance of BHJ devices (24, 28–33). Therefore, MEH-PPV, MDMO-PPV, and P3HT could be attributed to classic polymer donors and have been well-addressed in certain reviews (29–32).

Electron donor (D)−electron acceptor (A) interactions play a fundamental role in organic chemistry. The reactivities and physical properties of organic compounds largely depend on the strength of the D−A interactions. Among a variety of electron-accepting functionalities, 1,3,5-triazine (hereafter simply "triazine") is a fascinating and interesting π-electron-deficient aromatic compound. Triazine possesses the largest nucleophilic susceptibility among various nitrogen-containing heteroaromatic six-membered ring compounds (34). The π-electron deficiency of triazine is useful in organic synthesis, and 2,4,6-trichloro-1,3,5-triazine (cyanuric chloride) is a valuable reagent not only for synthesizing a lot of triazine derivatives but also as a coupling reagent in the formation of macrocyclic lactones (35) and β-lactams (36).

Very recently, we have synthesized low-band-gap vinylene compounds with triphenylamine and benzothiadiazole segments for use in PV cells (37). Moreover, we have synthesized low- band-gap *p*-phenylenevinylene compounds containing thiophene or anthracene moieties for PV applications (38). All these small molecules carried terminal cyanovinylene 4-nitrophenyls which broaden their absorption spectra. The BHJ solar cells, which were fabricated by blending the above small molecules with PCBM, gave PCE of 1.13−1.66 %, which was increased to 2.33−2.49 % upon thermal annealin g (37, 38).

In continuation of our research for preparing low-band-gap small molecules and polymers, we synthesized a star-shaped small molecule (**SM**) and an alternating *p*-phenylenevinylene copolymer (**P**) that contained cyanovinylene 4-nitrophenyl segments. The effect of these segments on the absorption spectra and the PV properties of **SM** and **P** were investigated. To the best of our knowledge, **P** is the first macromolecule that carries cyanovinylene 4-nitrophenyls and therefore its PV behavior is of interest, since other related polymers could be designed and synthesized. The PV properties of the BHJ devices based on **SM**:PCBM and **P**:PCBM have been investigated and the overall PCE for these devices were found approximately at 2.37 and 1.43 % for **SM**:PCBM and **P**:PCBM, respectively for the as cast films. The higher value of PCE for **SM**:PCBM has been attributed to the higher difference in the LUMO levels between **SM** and PCBM as compared to the difference in the LUMOs of **P** and PCBM and the relatively higher value of hole mobility. When thermally annealed **SM**:PCBM and **P**:PCBM active layers are used in the device, the PCE further increased up to 3.82 and 2.37 %, respectively. This can be explained with the analysis of XRD and optical microstructures. The fact that **SM**, which was synthesized by a simple two-step synthetic route utilizing inexpensive and highly available starting materials, afforded photovoltaic device with PCE of ∼4 %, must be seriously taken into account. In addition, our research functions as proof against the necessity of clear structure−property relations, in order to obtain high PCE in organic solar cells.

EXPERIMENTAL SECTION

Characterization Methods. IR spectra were recorded on a Perkin-Elmer 16PC FT-IR spectrometer with KBr pellets. ^{1}H NMR (400 MHz) spectra were obtained using a Brucker spectrometer. Chemical shifts (δ values) are given in parts per million with tetramethylsilane as an internal standard. UV−vis spectra were recorded on a Beckman DU-640 spectrometer with spectrograde THF. Elemental analyses were carried out with a Carlo Erba model EA1108 analyzer. Gel permeation chromatography (GPC) analysis was conducted with a Waters Breeze 1515 apparatus equipped with a 2410 differential refractometer as a detector (Waters Associate) and Styragel HR columns with polystyrene as a standard and tetrahydrofuran (THF) as an eluant.

The topographical images of the films were obtained from an optical micrograph system (Labomed optical microscope of 1 μm resolution) and were done under ambient conditions. The interlayer spacing was studied using the X-ray diffraction (XRD) technique. Thin film XRD spectra were recorded using a panalytical (XRD) system, with CuKα acting as the radiation source of wavelength $\lambda = 1.5405$ Å.

Reagents and Solvents. 1,4-Divinyl-2,5-bis(hexyloxy)-benzene (**6**) was prepared by Stille coupling reaction (39) of 1,4-dibromo-2,5-bis(hexyloxy)-benzene with tributylvinyltin (40). 4-Nitrobenzyl cyanide was synthesized from the nitration of benzyl cyanide with concentrated nitric and sulfuric acid (41). *N,N*-Dimethylformamide (DMF) and tetrahydrofuran (THF) were dried by distillation over CaH_2. Triethylamine was purified by distillation over KOH. All other reagents and solvents were commercially purchased and used as supplied.

Preparation of Monomer SM and copolymer P. ***4,4′,4″-[1,3,5-Triazine-2,4,6-triyltris(oxy)]tris-benzaldehyde (Compound 1).*** A flask was charged with a mixture of cyanuric chloride (0.25 g, 1.35 mmol), 4-hydroxybenzaldehyde (0.51 g, 4.17 mmol), *p*-dioxane (20 mL), and Na_2CO_3 (0.50 g, 4.72 mmol). The mixture was stirred and refluxed for 12 h under N_2. It was subsequently concentrated under reduced pressure and the concentrate was poured into cold water (10 mL). The precipitate was filtered off, washed with cold water (5 mL), and dried to afford **1** (0.20 g, 34 %).

Scheme 1. Synthesis of Monomer SM

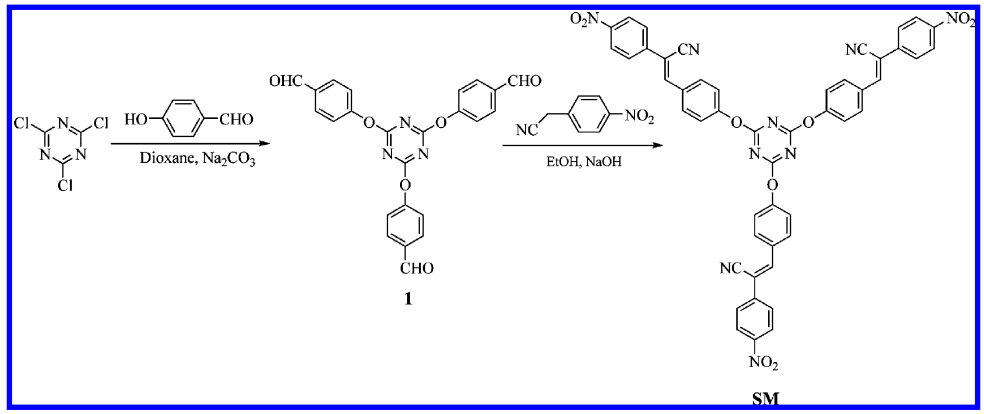

FT-IR (KBr, cm^{-1}): 3026, 1724, 1640, 1600, 1398, 1288, 1218, 1160, 1054, 834, 772.

^1H NMR ($CDCl_3$, ppm): 9.85 (s, 3H, CHO); 7.65 (d, 6H, phenylene meta to oxygen); 6.95 (d, 6H, phenylene ortho to oxygen).

Anal. Calcd for $C_{24}H_{15}N_3O_6$: C, 65.31; H, 3.43; N, 9.52. Found: C, 64.76; H, 3.48; N, 9.63.

***Monomer* SM.** A flask was charged with a solution of **1** (0.35 g, 0.79 mmol) and 4-nitrobenzyl cyanide (0.39 g, 2.37 mmol) in anhydrous ethanol (40 mL). Sodium hydroxide (0.19 g, 4.75 mmol) dissolved in anhydrous ethanol (20 mL) was added portionwise to the stirred solution. The mixture was stirred for 1 h at room temperature under N_2 and then concentrated under reduced pressure. Monomer **SM** precipitated as a dark green solid by cooling into refrigerator. It was filtered off, washed thoroughly with water, and dried. The crude product was recrystallized from DMF–water (3:1 v/v) (0.59 g, 85 %).

FT-IR (KBr, cm^{-1}): 2160, 1584, 1508, 1490, 1458, 1342, 1288, 1270, 1184, 1108, 852.

^1H NMR (DMSO-d_6, ppm): 8.23 (m, 6H, phenylene ortho to nitro); 7.76 (s, 3H, olefinic); 7.55 (m, 6H, phenylene meta to nitro); 7.25 (m, 6H, phenylene meta to oxygen); 6.93 (m, 6H, phenylene ortho to oxygen).

Anal. Calcd for $C_{48}H_{27}N_9O_9$: C, 65.98; H, 3.11; N, 14.43. Found: C, 64.25; H, 3.04; N, 14.26.

(Z)-3-(2,5-Dibromothiophen-3-yl)-2-(4-nitrophenyl)acrylonitrile (Compound 5). A flask was charged with a solution of **4** (1.22 g, 4.52 mmol) and 4-nitrobenzyl cyanide (0.73 g, 4.52 mmol) in anhydrous ethanol (50 mL). Sodium hydroxide (0.36 g, 9.00 mmol) dissolved in anhydrous ethanol (40 mL) was added portion-wise to the stirred solution. The mixture was stirred for 1 h at room temperature under N_2 and then was concentrated under reduced pressure. Compound **5** precipitated as a dark green solid by cooling into refrigerator. It was filtered off, washed thoroughly with water and dried. The crude product was purified by column chromatography, eluting with a mixture of dichloromethane and hexane (1:1) (1.60 g, 86 %).

FT-IR (KBr, cm^{-1}): 2180, 1584, 1522, 1508, 1490, 1290, 1184, 1108, 1058, 852.

^1H NMR ($CDCl_3$, ppm): 8.10 (d, 2H, phenylene ortho to nitro); 7.74 (s, 1H, olefinic); 7.53 (d, 2H, phenylene meta to nitro); 7.10 (s, 1H, thiophene).

Anal. Calcd for $C_{13}H_6Br_2N_2O_2S$: C, 37.71; H, 1.46; N, 6.77. Found: C, 36.12; H, 1.13; N, 6.35.

Copolymer P. A flask was charged with a mixture of **5** (0.2360, 0.570 mmol), 1,4-divinyl-2,5-bis(hexyloxy)benzene (6) (0.1885 g, 0.570 mmol), $Pd(OAc)_2$ (0.0053 g, 0.024 mmol), P(*o*-tolyl)$_3$ (0.0399 g, 0.131 mmol), DMF (5 mL) and triethylamine (3 mL). The flask was degassed and purged with N_2. The mixture was heated at 90 °C for 24 h under N_2. It was then filtered and the filtrate was poured into methanol. The precipitate was filtered and washed with methanol. The crude product was purified by dissolution in THF and precipitation in methanol (0.2392 g, 72 %).

FT-IR (thin film on NaCl cell, cm^{-1}): 3054, 2952, 2930, 2868, 2160, 1588, 1492, 1464, 1344, 1288, 1208, 1106, 960, 852, 752.

^1H NMR ($CDCl_3$, ppm): 8.26 (m, 2H, phenylene ortho to nitro); 7.70 (m, 1H, cyano-olefinic); 7.45 (m, 2H, phenylene meta to nitro); 7.33 9 (d, 4H, olefinic); 7.12 (s, 1H, thiophene); 6.96 (m, 2H, phenylene ortho to oxygen); 3.94 (m, 4H, $OCH_2(CH_2)_4CH_3$); 1.78 (m, 4H, $OCH_2CH_2(CH_2)_3CH_3$); 1.46 (m, 12H, $O(CH_2)_2(CH_2)_3CH_3$); 0.92 (t, 6H, $O(CH_2)_5CH_3$).

Anal. Calcd for $(C_{35}H_{38}N_2SO_4)_n$: C, 72.13; H, 6.57; N, 4.81. Found: C, 71.58; H, 6.32; N, 4.27.

Device Fabrication and Characterization. The polymer PV devices were fabricated on patterned indium tin oxide (ITO) coated glass substrate, which had been cleaned by successive ultrasonic treatment in acetone and isopropyl alcohol and then dried at 80 °C for 30 min. A 50 nm thick poly(ethylenedioxythiophene):poly(styrene sulfonate) (PEDOT:PSS) layer was spin-coated onto the ITO glass and baked at 120 °C for 15 min in ambient. A 80 nm thick **P**:PCBM or **SM**:PCBM blend layer in THF solution was deposited on the top of the PEDOT:PSS layer by controlled spin-coating rate. Finally, the substrates were transferred into a thin film coating unit to deposit 50 nm thick aluminum (Al) electrodes, producing an active layer of 0.15 cm^2 for each device. A mask with area of 0.15 cm^2 was used during the thermal evaporation of the Al electrode. Prethermal annealing of the active layers was carried out at 100 °C for 2 min on the hot plate before the deposition of Al electrode.

Current–voltage (J–V) characteristics of the PV devices were measured using a computer controlled Keithley 238 source meter under illumination intensity of 100 mW/cm^2. A 100 W halogen lamp without solar simulator was used as light source. The J–V characteristic measurements under illumination were carried out in a dark chamber (wooden box) with a window slit of 2 cm^2 area for illumination. The hole only device having ITO/PEDOT:PSS/**SM**:PCBM or **P**:PCBM/Au configuration using as cast and thermally annealed active layers, were fabricated and the J–V characteristics in dark at room temperature, were recorded to estimate the hole and electron mobility of the blended layer using the SCLC model.

RESULTS AND DISCUSSION

Synthesis and Characterization. Scheme 1 outlines the synthesis of monomer **SM**. In particular, cyanuric chloride reacted with 4-hydroxybenzaldehyde in *p*-dioxane in the presence of Na_2CO_3 to afford compound **1**. The latter reacted with 4-nitrobenzyl cyanide in anhydrous ethanol in the

Scheme 2. Synthesis of Copolymer P (NBS, *N*-bromosuccinimide; BPO, benzoyl peroxide; HMT:, hexamethylenetetramine)

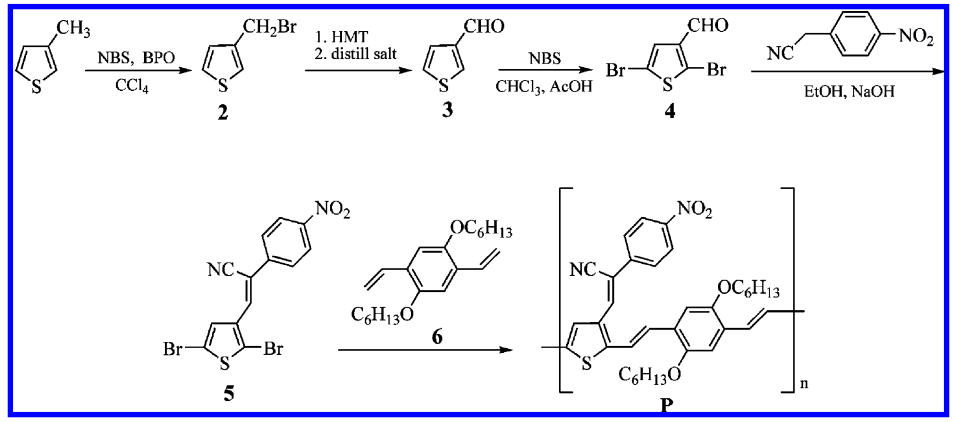

presence of NaOH to yield **SM**. This monomer was soluble only in strongly polar solvents with a high boiling point, such as DMF and dimethylsulfoxide (DMSO).

Scheme 2 presents the five-step reaction sequence applied for the synthesis of copolymer **P**. Specifically, compounds **2** (42), **3** (43), and **4** (44) were prepared according to the literature. The reaction of **4** with 4-nitrobenzyl cyanide in anhydrous ethanol in the presence of NaOH gave the key-monomer **5**. Finally, the Heck coupling of **5** with **6** afforded the target copolymer **P**. This reaction took place in DMF utilizing palladium acetate as catalyst and triethylamine as an acid scavenger. The Heck reaction is known to produce mixture of trans, cis, or α fashion couplings (45). Moreover, this polymerization method gives no regioselectivity of the coupling direction, resulting in a regiorandom product in terms of the cyanovinylene position on the thiophene units. The hexyloxy side chains enhanced the solubility of **P**, which was very soluble in common organic solvents, like THF, chloroform, and dichloromethane. The preparation yield of **P** after the purification process was 72% and the number average molecular weight (M_n) was 9600, by GPC, with a polydispersity of 2.6.

Structural characterization of **SM** and **P** was accomplished by FT-IR and ^{1}H NMR spectroscopy. The FT-IR and ^{1}H NMR spectra of **SM** and **P** were consistent with their chemical structures (see the Supporting Information).

Photophysical Properties. Figure 1 presents the UV−vis absorption spectra of **SM** and **P** both in dilute (1×10^{-5} M) THF solution and thin film. They are normalized with respect the long-wavelength peak. All photophysical characteristics are summarized in Table 1.

The absorption spectra of **SM** were broad and extended from 300 up to ~800 nm with long-wavelength maximum ($\lambda_{a,max}$) at 648 nm. The thin film absorption onset of **SM** was located at 793 nm which corresponds to an optical band gap (E_g^{opt}) of 1.57 eV. **SM** contains an ether linkage between triazine and benzene rings. This would break the π-conjugation and weaken the electronic interaction between the peripheral groups and the core. The absorption spectra of **P** were somewhat less broad than those of **SM** and extended from 300 up to ~750 nm. Their $\lambda_{a,max}$ was at the range of 630−645 nm and is attributable to an intramolecular charge transfer (ICT) between the electron-donating thiophene dihexyloxyphenylenevinylene and the electron-withdrawing cyanovinylene 4-nitrophenyl. The thin film absorption onset of **P** was located at 730 nm corresponding to an E_g^{opt} of 1.70 eV. The absorption spectra of **SM** and **P** showed a reduced absorption intensity around 550 nm which was more pronounced for **P**. The E_g^{opt} of the present samples are comparable with those (1.65−1.71 eV) of other related materials, which have been prepared in our laboratory (37, 38). The lower E_g^{opt} for **SM** as compared to **P** demonstrates that the three branched start type compound **SM** has stronger absorption ability than copolymer **P**.

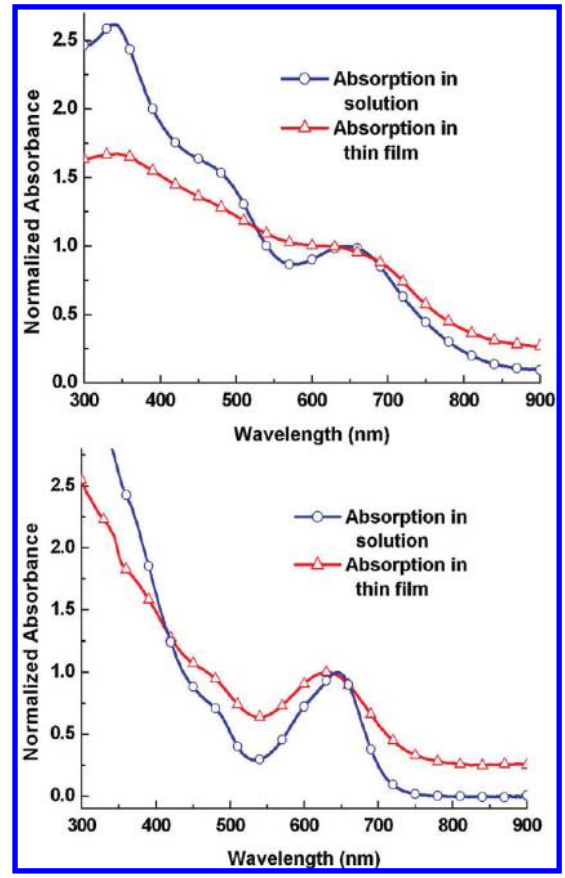

FIGURE 1. Normalized UV−vis absorption spectra in THF solution and thin film of small molecule SM (top) and copolymer P (bottom).

Table 1. Optical and Electrochemical Properties of SM and P

	SM	P
$\lambda_{a,max}$[a] in solution (nm)	648	645
$\lambda_{a,max}$[a] in thin film (nm)	648	630
E_g^{opt}[b](eV)	1.57	1.70
E_{onset}^{red} (V)	−1.10	−1.06
E_{onset}^{ox} (V)	0.50	0.70
HOMO (eV)	−5.2	−5.4
LUMO (eV)	−3.6	−3.65
E_g^{el}[c] (eV)	1.60	1.75

[a] $\lambda_{a,max}$: The absorption maxima from the UV−vis spectra in THF solution or in thin film. [b] E_g^{opt}: Optical band gap determined from the absorption onset in thin film. [c] E_g^{el}: Electrochemical band gap determined from cyclic voltammetry.

Electrochemical Properties. To determine the highest occupied molecular orbital (HOMO) and lowest unoccupied molecular orbital (LUMO) levels of **SM** and **P**, we carried out electrochemical cyclic voltammetry for both **SM** and **P** film on a glassy carbon electrode (see the Supporting Information). The potentials were internally calibrated for Ag/AgCl, which is estimated to have an oxidation potential of −4.71 eV vs vacuum. The cyclic voltammetry of both materials shows that there are a couple of reversible oxidation peaks in positive potential region, and an irreversible reduction peak in the negative potential. The HOMO (E_{HOMO}) and LUMO (E_{LUMO}) levels were estimated from the onset oxidation (E_{onset}^{ox})and reduction potential (E_{onset}^{red}) according to following equations

$$E_{HOMO} = -e(E_{onset}^{ox} - 4.71)\ \text{eV}$$

$$E_{LUMO} = -e(E_{onset}^{red} - 4.71)\ \text{eV}$$

where the unit of potential is V vs Ag/AgCl (46).

The onset oxidation and reduction potentials for both **P** and **SM** obtained from cyclic voltammetry are summarized in Table 1. Moreover, their HOMO and LUMO energy levels are shown in this table. In comparison with the HOMO level of −6.3 eV and the LUMO level of −4.1 eV for PCBM, both **SM** and **P** are suitable for use as donor materials blended with PCBM as acceptor in organic BHJ solar cells. The electrochemical band gaps (E_g^{elc}) were 1.60 eV for **SM** and 1.75 eV for **P** which are slightly higher than the corresponding E_g^{opt} values (Table 1). The slightly higher value of LUMO for **SM** as compared to the **P** may be attributed to the change in the observed onset reduction potential value.

Electrical Properties of SM and P. Panels a and b in Figure 2 show the $J-V$ characteristics of the devices based on **SM** and **P** thin films sandwiched between ITO/PEDOT:PSS and Al electrodes, in dark as well as under illumination intensity of 100 mW/cm^2, at room temperature. The $J-V$ characteristics of both devices, in dark show a rectification effect, when positive potential is applied to PEDOT:PSS-coated ITO electrode with respect to the Al electrode. Because the work function of PEDOT:PSS coated on ITO (5.2 eV) is very close to the HOMO level of the **SM** (−5.2 eV) and **P** (−5.4 eV), this electrode behaves as nearly Ohmic contact

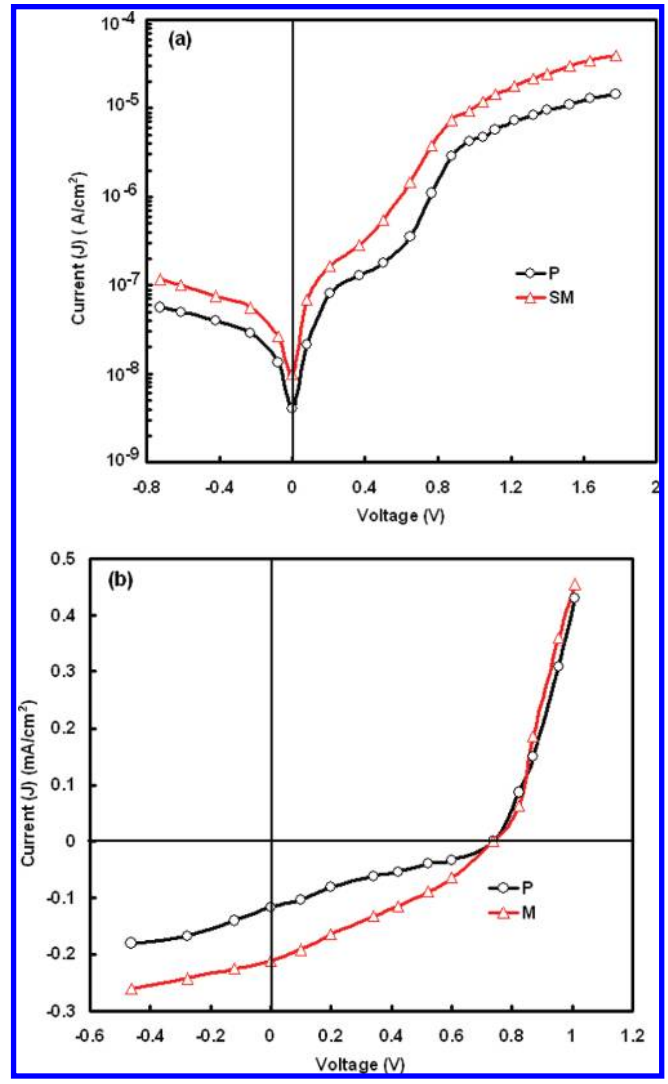

FIGURE 2. Current−voltage characteristics of devices based on SM and P in (a) dark and (b) under illumination intensity of 100 mW/cm^2; the active layer is sandwiched between ITO/PEDOT:PSS and Al electrode.

for hole injection from electrode into the HOMO level of small molecules. However, the LUMO level of both materials is very far from the work function of Al (4.2 eV) and forms the Schottky barrier for the electron injection from Al into the LUMO level of the organic compounds. Therefore, the rectification effect is due to the formation of Schottky barrier at the Al-organic layer interface.

The charge carrier mobility of the PV materials is also an important factor which influences the performance of organic solar cells. The hole mobilities of **SM** and **P** were measured using the space charge limited current (SCLC) method (47–49) with the device structure ITO/PEDOT:PSS/**SM** or **P**/Au. The $J-V$ characteristics of the devices were plotted as $\ln(Jd^3/(V_{appl} - V_{bi}))$ versus $[(V_{appl} - V_{bi})/d]^{0.5}$, as shown in Figure 3. The hole mobilities of **SM** and **P** calculated from the intercepts of corresponding lines are 2.3×10^{-5} and 7.6×10^{-6} cm^2/(V s), respectively. Because the building blocks of **SM** and **P** are quite different, their hole mobilities can not be compared. The PCE of the PV devices fabricated with **SM** and **P** were estimated from the $J-V$ characteristics

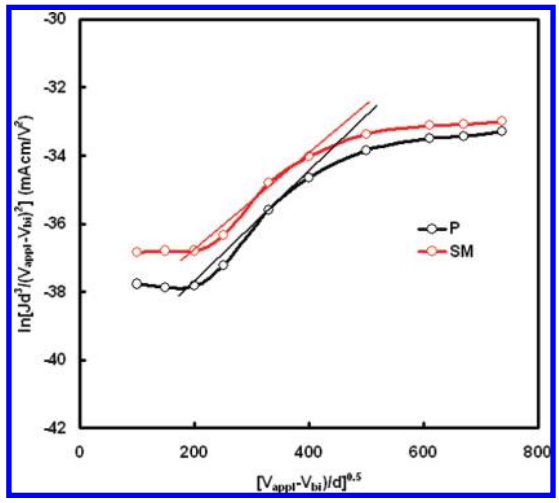

FIGURE 3. Current−voltage characteristics data from the ITO/PEDOT:PSS/P or SM/Au devices, plotted in the form of $\ln[Jd^3/(V_{appl} - V_{bi})^2]$ vs $[(V_{appl} - V_{bi})/d]^{0.5}$.

Table 2. Photovoltaic Parameters of Single-Layer Devices Using Only SM and P

device	short circuit current (J_{sc}) (mA/cm^2)	open circuit voltage (V_{oc}) (V)	fill factor (FF)	power conversion efficiency (η) (%)
ITO/PEDOT:PSS/**SM**/Al	0.21	0.74	0.32	0.05
ITO/PEDOT:PSS/**P**/Al	0.10	0.73	0.28	0.02

under illumination, as shown in Figure 2b, and are summarized in Table 2. It can be seen from this table that the short circuit current (J_{sc}) is higher for the device based on **SM** as compared to the **P**, under the same conditions. This feature may be attributed to the lower band gap and higher hole mobility of **SM** compared to **P**, as described earlier, and we believe that they are responsible for the higher PCE.

Photovoltaic Studies Based on Bulk Heterojunction. We have fabricated the BHJ organic PV devices based on **SM**:PCBM and **P**:PCBM blend with different ratios of donor and acceptor, but we found that the blends with 1:1 ratio by weight gives the best performance. The BHJ organic solar cells were fabricated with spin-cast blend films of **SM**:PCBM or **P**:PCBM (1:1 w/w) active layer and Al as the cathode. Figure 4 shows the current voltage characteristics of the devices in dark and under illumination intensity of 100 mW/cm^2. The PV parameters of both devices are summarized in Table 3. As it can be seen from this table, the device based on **SM**:PCBM blend shows better PV response having PCE 2.57 % as compared to the 1.43 % for the device based on **P**:PCBM. The incident photon to current efficiency (IPCE) spectra of the devices (Figure 5) shows similar shape to the absorption spectra of the corresponding blends employed in the devices, indicating that all the visible light absorption of **SM** and **P** contributes to J_{sc}. The maximum value of IPCE for **SM**:PCBM and **P**:PCBM based devices are about 55 and 35 %, respectively. The IPCE values are consistent with higher values of J_{sc} and PCE of the **SM**:PCBM-based organic solar cell. The optical microstructure images of the **SM**:PCBM and **P**:PCBM blends, which are

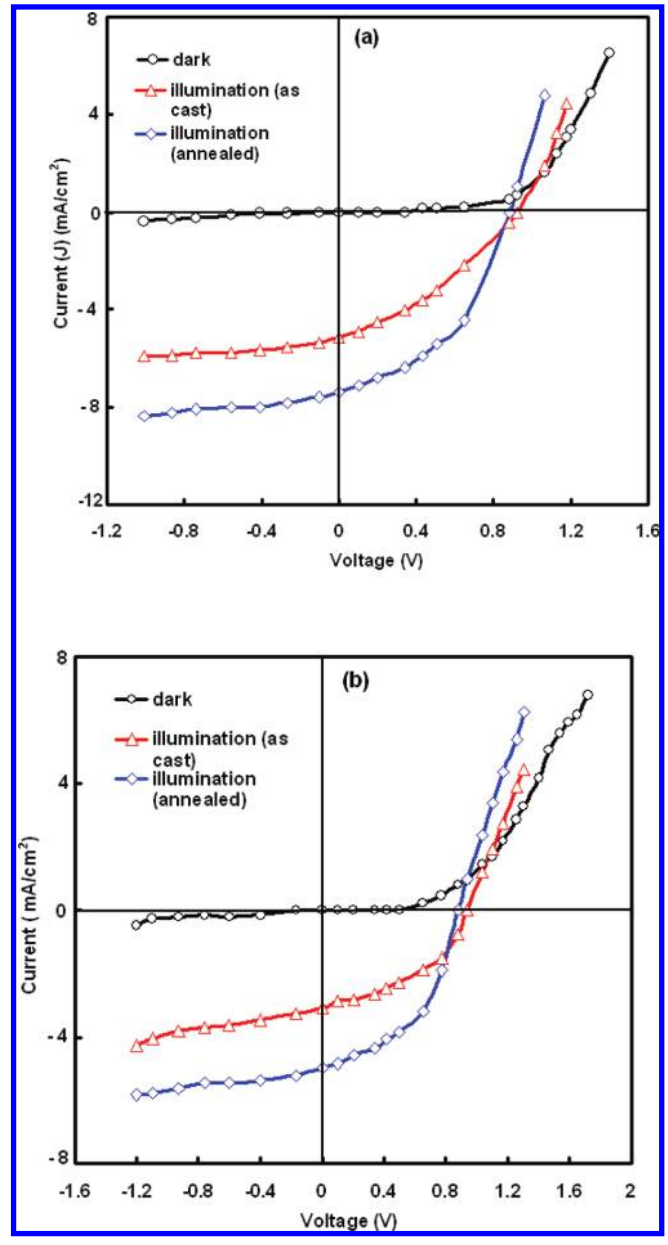

FIGURE 4. Current−voltage characteristics of bulk heterojunction devices based on (a) SM:PCBM (1:1) and (b) P:PCBM (1:1) in dark and under illumination.

shown in Figure 6, reveal that **SM** has better film forming property as compared to **P**. The higher PCE of the device with **SM** as donor was attributed to its relatively lower band gap, higher hole mobility, and better quality of the film.

The photocurrent in BHJ PV device is determined by the product of the absorbed photons within the solar spectrum and the IQE of the device (23, 50, 51). As can be seen from Figure 1 and Table 1, the optical absorption spectra and optical band gap are different for **SM** and **P**. Consequently, the photon absorbed in both active layers are different. The other factor for the difference in the photocurrent is also attributed to the difference in the IQE of the devices. The IQE is determined by three processes: (a) migration/diffusion of photogenerated excitons to the D/A interface, (b) excitons dissociation and charge separation at the interfaces, and (c) collection of charge carriers at ITO and Al electrodes. The

Table 3. Photovoltaic Parameters of BHJ Devices Using SM:PCBM (1:1) and P:PCBM (1:1) Active Layers, Sandwiched between ITO/PEDOT:PSS and Al Electrodes

device	short circuit current (J_{sc}) (mA/cm^2)	open circuit voltage (V_{oc}) (V)	fill factor (FF)	power conversion efficiency (η) (%)
ITO/PEDOT:PSS/**SM**:PCBM (as cast)/Al	5.1	0.92	0.54	2.53
ITO/PEDOT:PSS/**SM**:PCBM (annealed)/Al	7.4	0.89	0.58	3.82
ITO/PEDOT:PSS/**P**:PCBM (as cast)/Al	3.11	0.94	0.49	1.43
ITO/PEDOT:PSS/**P**:PCBM (annealed)/Al	4.98	0.88	0.54	2.37

process (a) depends upon the nanoscale phase separation between the donor and acceptor materials used in the BHJ active layer. It can be seen that the topographical image (Figure 6) for the **SM**:PCBM is more uniform than that for **P**:PCBM, which indicates better nanoscale phase separation of the active layer for **SM**:PCBM. Therefore, we assume that the contribution for IQE from process a is higher for **SM**:PCBM. For process b, a sufficiently large energy difference between the LUMO of donor and acceptor material is required for ultrafast photoinduced charge transfer. This difference is bigger for the **SM:**PCBM (0.4 eV) as compared to **P**:PCBM (0.35 eV) blend and the photoinduced charge transfer is slightly faster in the former blend, resulting in higher IQE for the device based on **SM:**PCBM. Process c depends on the percolated path for electrons and holes in the BHJ active layer and depends also on the position of HOMO and LUMO of donor and acceptor materials respective, relative to the work function of anode the cathode. The HOMO level of the **SM** is closer to the HOMO of PEDOT:PSS, which results in more efficient hole collection. Therefore, processes a−c are responsible for the improved J_{sc} and PCE of the device based on the **SM**:PCBM blend.

Effect of Thermal Annealing. Generally, the performance of BHJ solar cells can be maximized by controlling the morphology of the blend active layer, because efficient photoinduced charge generation, transport, and collection at each electrode crucially depend on the nanometer scale morphology of the blend films (52, 53). The crystallization of polymer improves the light-harvesting property by extending the conjugation length and increases hole mobility, which is the limiting factor for the balance transport of charges dissociated from the bound excitons (30). An ordered BHJ morphology can be achieved by the interdiffusion of each molecule in the blend films. It has been reported that thermal annealing of the polymer:PCBM blend films can induce isolated PCBM molecules diffusing into large aggregates or increases the demixing between polymer and PCBM components (54, 55). Here, we have subjected the blend layer of **SM**:PCBM or **P**:PCBM to thermal annealing before the deposition of final Al electrode and the $J-V$ characteristics of the devices in dark and under illumination of 100 mW/cm^2 were recorded and are shown in Figure 4. The PV parameters are summarized in Table 3. The IPCE values of the devices (Figure 5) based on the thermally annealed films also increases, which is inconsistent with the observed value of J_{sc}. The overall power conversion efficiencies of the devices were found to increase upon thermal annealing of active layer, which is mainly due to the increase in J_{sc} and fill factor of the devices.

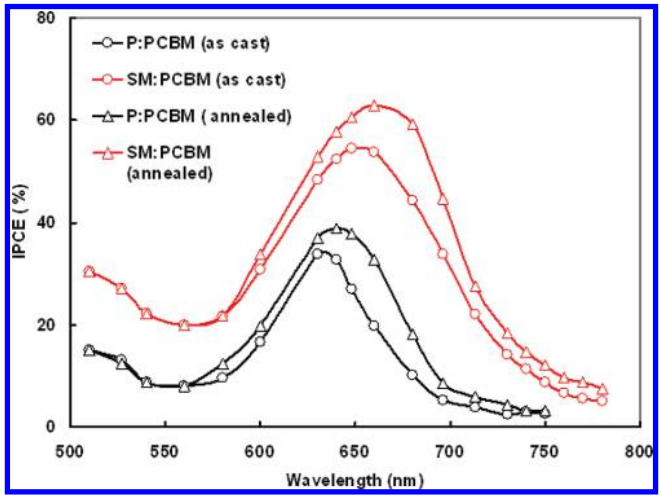

FIGURE 5. IPCE spectra of the bulk heterojunction solar cells based on P:PCBM or SM:PCBM blend active layers.

The thermal annealing of **SM**:PCBM or **P**:PCBM blend film improves the light absorption by extending the conjugation length, and charge transport, by increasing the hole mobility of **P** or **SM**. These results can mainly attribute to the improved crystallinity morphology of **SM** or **P**, which can easily self organize into well-ordered chains during solidification from a wet film. Generally, the degree of crystallinity in **SM** or **P** films can be evaluated by examining the UV−visible absorption spectra, in which well-organized structure of **SM** or **P** is confirmed by a red shift in the absorption peak and increased intensity.

To get information about the change in the hole mobility in the blended active layer upon thermal annealing, the $J-V$ characteristics of the hole only device was measured for the as cast and thermally annealed blended layers. The hole mobility was extracted using the SCLC model for $J-V$ characteristics in dark at room temperature as discussed earlier. The as cast active layers of **SM**:PCBM and **P**:PCBM exhibit the hole mobilities as observed in pure **SM** and **P**, respectively. However, when the blends are thermally annealed, the hole mobility in both blends increases by one order of magnitude (1.9×10^{-4} cm^2/(V s) and 8.5×10^{-5} cm^2/(V s) for **SM** and **P**, respectively). The carrier mobility was found to be more balanced for the thermally annealed active layer than that for the as cast film and may be one of the factors that contribute to higher device performance.

We have also examined the effect of thermal annealing on the surface structure of both **SM**:PCBM and **P**:PCBM blends. Figure 6 shows the topographic images of the as cast and thermally annealed films. It can be seen from these images

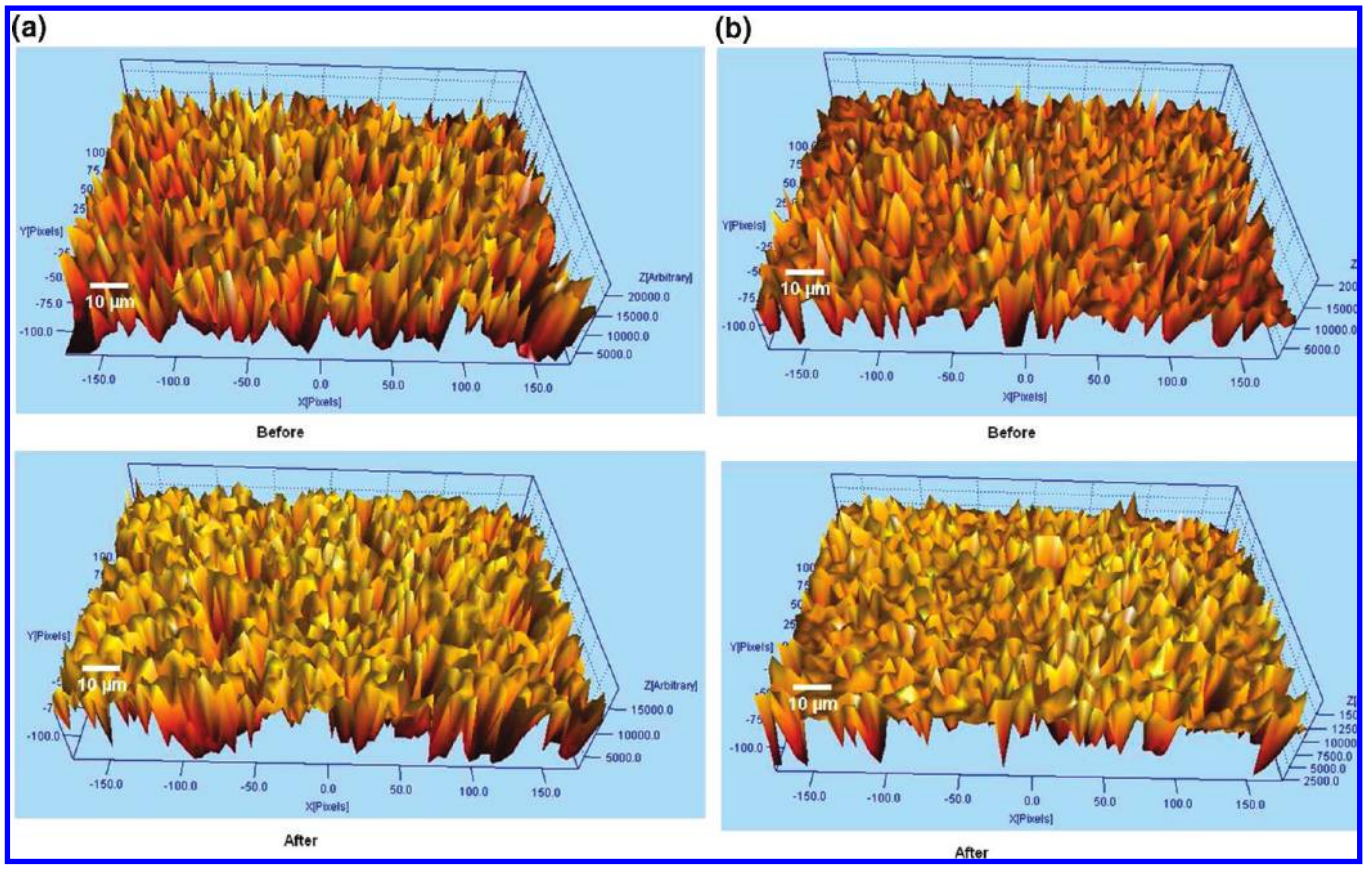

FIGURE 6. (a) Optical topographical images of SM:PCBM films before and after thermal annealing. (b) Optical topographical images of P:PCBM blends films before and after thermal annealing.

that there is a significant change in the microscopic structure for the thermally annealed blend as compared to the as cast blend. This feature also indicates that crystallinity of **P** and **SM** increased upon thermal annealing. This increase in crystallinity results in an increased interfacial area for photoinduced charge transfer, and thereby enhances the photocurrent.

Thin film XRD was used to determine the differences in crystallinity of the pure and blended films before and after thermal annealing. Figure 7 gives the diffraction patterns of the as cast and annealed pure film and the blends. As seen in Figure 7, the pure **SM** film exhibits a peak centered at $2\theta = 7.0°$, corresponding to an interplanar distance of 16.2 A. Annealing leads to higher peak intensity, indicating a higher degree of crystallinity. The diffraction peak of the **SM**:PCBM film (Figure 7) is centered at $2\theta = 7.4°$, corresponding to an interplanar distance of 15.8 Å. Similar results have been recorded for the **P**:PCBM films. The diffraction intensity of the thermally annealed blend also increases. These changes in the film crystallinity after thermal annealing agree with what is observed in the absorption spectra. Because most of the fullerene acceptors, such as PCBM, do not show any diffraction patterns in the range of 2θ values used (56), the changes in crystallinity of the blended film after thermal annealing are mainly attributed to an increase in crystallite size of the **SM** donor material. The increase in the crystallinity of **SM** upon thermal annealing leads to an improvement in the hole mobility that increases the overall PCE.

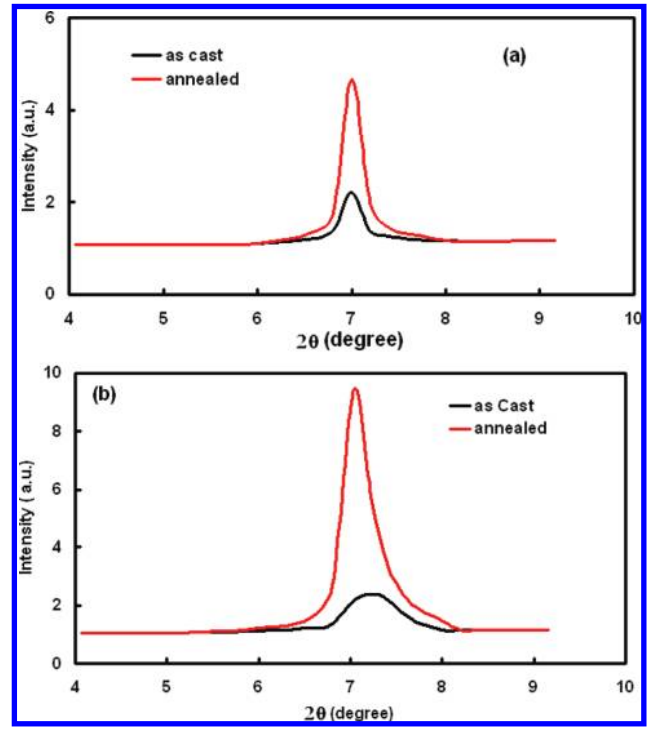

FIGURE 7. XRD patterns for the as cast and annealed (a) pure SM and (b) SM:PCBM thin films.

CONCLUSIONS

A small molecule **SM** and a copolymer **P** having common structural features, such as cyanovinylene 4-nitrophenyls, were synthesized. **SM** dissolved only in strongly polar solvents,

whereas **P** was very soluble in common organic solvents. Both displayed broad absorption spectra with long-wave maximum at 630−648 nm and optical band gap of 1.57−1.70 eV. PV devices have been fabricated with pure **SM**, **P**, **SM:**PCBM and **P:**PCBM active layers. It was found that the overall PCE of the device based on pure **SM** is higher than that for pure **P**, and this was attributed to the higher hole mobility in **SM** as compared to that in **P**. Moreover, the PCE of the PV device based on the **SM**:PCBM blend active layer is higher than that of the **P**:PCBM. This behavior was attributed to the higher difference in between the LUMO levels of **SM** and PCBM as compared to that for copolymer **P**-based blend. The improvement in PCE with the device based on thermally annealed films has been explained in terms of an increase in surface roughness and crystallinity of the active layer upon thermal annealing, as was analyzed from the optical microstructure and the XRD patterns of the thin films. The PCE was approximately 3.82 and 2.37% for **SM:**PCBM and **P:**PCBM-1based devices, respectively. These results are preliminary based on the illumination without using a solar simulator.

Supporting Information Available: Structural characterization of small molecule **SM** and copolymer **P** by FT-IR and ^{1}H NMR spectroscopy; ^{1}H NMR spectrum of copolymer **P**; information about the CV measurements of the materials (PDF). This material is available free of charge via the Internet at http://pubs.acs.org.

REFERENCES AND NOTES

(1) For a review see: Bundgaard, E.; Krebs, F. C. *Sol. Energy. Mater. Sol. Cells* **2007**, *91*, 954–985.
(2) Dhanabalan, A.; van Duren, J. K. J.; van Hal, P. A.; van Dongen, J. L. J.; Janssen, R. A. J. *Adv. Funct. Mater.* **2001**, *11*, 255–262.
(3) Wang, X.; Perzon, E.; Delgado, J. L.; De la Cruz, P.; Zhang, F.; Langa, F.; Andersson, M. R.; Inganäs, O. *Appl. Phys. Lett.* **2004**, *85*, 5081–5083.
(4) Inganäs, O.; Svensson, M.; Zhang, F.; Gadisa, A.; Persson, N. K.; Wang, X.; Andersson, M. R. *Appl. Phys. A* **2004**, *79*, 31–35.
(5) Campos, L. M.; Tontcheva, A.; Guenes, S.; Sonmez, G.; Neugebauer, H.; Sariciftci, N. S.; Wudl, F. *Chem. Mater.* **2005**, *17*, 4031–4033.
(6) Zhang, F.; Mammo, W.; Andersson, L. M.; Admassie, S.; Andersson, M. R.; Inganäs, O. *Adv. Mater.* **2006**, *18*, 2169–2173.
(7) Wienk, M. M.; Struijk, M. P.; Janssen, R. A. J. *Chem. Phys. Lett.* **2006**, *422*, 488–491.
(8) Wienk, M. M.; Turbiez, M. G. R.; Struijk, M. P.; Fonrodona, M.; Janssen, R. A. J. *Appl. Phys. Lett* **2006**, *88*, 153511/1–153511/3.
(9) Mühlbacher, D.; Scharber, M.; Morana, M.; Zhu, Z.; Waller, D.; Gaudiana, R.; Brabec, C. *Adv. Mater.* **2006**, *18*, 2884–2889.
(10) Peet, J.; Kim, J. Y.; Coates, N. E.; Ma, W. L.; Moses, D.; Heeger, A. J.; Bazan, G. C. *Nat. Mater.* **2007**, *6*, 497–500.
(11) Colladet, K.; Fourier, S.; Cleij, T. J.; Lutsen, L.; Gelan, J.; Vanderzande, D.; Nguyen, L. H.; Neugebauer, H.; Sariciftci, S.; Aguirre, A.; Janssenand, G.; Goovaerts, E. *Macromolecules* **2007**, *40*, 65–72.
(12) Perzon, E.; Zhang, F.; Andersson, M.; Mammo, W.; Inganäs, O.; Andersson, M. R. *Adv. Mater.* **2007**, *19*, 3308–3311.
(13) Wienk, M. M.; Turbiez, M.; Gilot, J.; J.; Janssen, R. A. *Adv. Mater.* **2008**, *20*, 2556–2560.
(14) Thompson, B. C.; Kim, Y.-G.; McCarley, T. D.; Reynolds, J. R. *J. Am. Chem. Soc.* **2006**, *128*, 12714–12725.
(15) Hou, J.; Chen, H.-Y.; Zhang, S.; Li, G.; Yang, Y. *J. Am. Chem. Soc.* **2008**, *130*, 16144–16145.
(16) Zoombelt, A. P.; Fonrodona, M.; Turbiez, M. G. R.; Wienk, M. M.; Janssen, R. A. J. *J. Mater. Chem.* **2009**, *19*, 5336–5342.
(17) Scharber, M. C.; Mühlbacher, D.; Koppe, M.; Denk, P.; Waldauf, C.; Heeger, A. J.; Brabec, C. J. *Adv. Mater.* **2006**, *18*, 789–794.
(18) Koster, L. J. A.; Mihailetchi, V. D.; Blom, P. W. M. *Appl. Phys. Lett* **2006**, *88*, 093511/1−093511/3.
(19) Roquet, S.; Cravino, A.; Leriche, P.; Aleveque, O.; Frere, P.; Roncali, J. *J. Am. Chem. Soc.* **2006**, *128*, 3459–3466.
(20) Tamayo, A. B.; Walker, B.; Nguyen, T. Q. *J. Phys. Chem. C* **2008**, *112*, 11545–11551.
(21) Lloyd, M. T.; Mayer, A. C.; Subramanian, S.; Mourney, D. A.; Herman, D. J.; Bapat, A.; Anthony, J. E.; Malliaras, G. G. *J. Am. Chem. Soc.* **2007**, *129*, 9144–9149.
(22) Valentini, L.; Bagnis, D.; Marrocchi, A.; Seri, M.; Taticche, A.; Kenny, J. M. *Chem. Mater.* **2008**, *20*, 32–34.
(23) Lloyd, M. T.; Anthony, J. E.; Malliaras, G. G. *Mater. Today* **2007**, *10*, 34–41.
(24) Hoppe, H.; Sariciftci, N. S. *J. Mater. Chem.* **2006**, *16*, 45–61.
(25) Shaheen, S.; Brabec, C. J.; Sariciftci, N. S.; Padinger, F.; Fromherz, T.; Hummelen, J. C. *Appl. Phys. Lett.* **2001**, *78*, 841–843.
(26) Zheng, L.; Zhou, Q.; Deng, X.; Yuan, M.; Yu, G.; Cao, Y. *J. Phys. Chem. B* **2004**, *108*, 11921–11926.
(27) Wang, L.; Liu, Y.; Jiang, X.; Qin, D.; Cao, Y. *J. Phys. Chem. C* **2007**, *111*, 9538–9542.
(28) Kim, J. Y.; Lee, K.; Coates, N. E.; Moses, D.; Nguyen, T.-Q.; Dante, M.; Heeger, A. J. *Science* **2007**, *317*, 222–225.
(29) Gunes, S.; Neugebauer, H. S.; Sariciftci, N. S. *Chem. Rev.* **2007**, *107*, 1324–1338.
(30) Coakley, K.; McGehee, M. D. *Chem. Mater.* **2004**, *16*, 4533–4542.
(31) Brabec, C. J.; Sariciftci, N. S.; Hummelen, J. C. *Adv. Funct. Mater.* **2001**, *11*, 15–26.
(32) Thompson, B. C.; Frechet, J. M. J. *Angew. Chem., Int. Ed.* **2008**, *47*, 58–77.
(33) Li, Y.; Zou, Y. *Adv. Mater.* **2008**, *20*, 2952–2958.
(34) Katritzky, A. R.; Rees, C. W.; Scriven, E. F. V. In *Comprehensive Heterocyclic Chemistry II*; Boulton, A. J., Ed.; Pergamon: New York, 1996; Vol. 6, Chapter 6.12.
(35) Cossy, J.; Pete, J. P. *Tetrahedron Lett.* **1986**, *27*, 2369–2370.
(36) Huang, H.; Wu, S. *Gaodeng Xuexiao Huaxue Xuebao* **1987**, *8*, 341–343.
(37) Mikroyannidis, J. A.; Stylianakis, M. M.; Suresh, P.; Balraju, P.; Sharma, G. D. *Org. Electron.* **2009**, *10*, 1320–1333.
(38) Mikroyannidis, J. A.; Stylianakis, M. M.; Balraju, P.; Suresh, P.; Sharma, G. D. *ACS Appl. Mater. Interfaces* **2009**, *1*, 1711–1718.
(39) McKean, D. R.; Parrinello, G.; Renaldo, A. F.; Stille, J. K. *J. Org. Chem.* **1987**, *52*, 422–424.
(40) Peng, Q.; Li, M.; Tang, X.; Lu, S.; Peng, J.; Cao, Y. *J. Polym. Sci., Part A: Polym. Chem.* **2007**, *45*, 1632–1640.
(41) Robertson, G. R. In *Organic Syntheses*; Gilman, H., Ed.; Wiley: New York, 1941; Collective Vol. 1, p 396.
(42) Zou, Y.; Wu, W.; Sang, G.; Yang, Y.; Liu, Y.; Li, Y. *Macromolecules* **2007**, *40*, 7231–7237.
(43) Campaigne, E.; Bourgeois, R. C.; McCarthy, W. C. In *Organic Syntheses*; Price, C. C., Dudley, E. A., Eds.; Wiley: New York, 1963; Vol. 4, p 918.
(44) van Beek, R.; Zoombelt, A. P.; Jenneskens, L. W.; van Walree, C. A.; Donegla, C. M.; Veldman, D.; Janssen, R. A. J. *Chem.—Eur. J.* **2006**, *12*, 8075–8083.
(45) Loewe, R. S.; McCullough, R. D. *Chem. Mater.* **2000**, *12*, 3214–3221.
(46) Hou, J.; Tan, Z.; Yan, Y.; He, Y.; Yang, C.; Li, Y. *J. Am. Chem. Soc.* **2006**, *128*, 4911–4916.
(47) Chirvase, D.; Chiguvare, Z.; Knipper, M.; Parisi, J.; Dyakonov, V.; Hummelen, J. C. *J. Appl. Phys.* **2003**, *93*, 3376–3383.
(48) Malliaras, G. G.; Salem, J. R.; Brock, P. J.; Scott, C. *Phys. Rev. B* **1998**, *58*, R13411–R13414.
(49) Martens, H. C. F.; Brom, H. B.; Blom, P. W. M. *Phys. Rev. B* **1999**, *60*, R8489–R8492.
(50) Schilinsky, R.; Waldauf, C.; Brabec, C. J. *Appl. Phys. Lett.* **2002**, *81*, 3885–3887.
(51) Hoppe, H.; Sariciftci, N. S. *J. Mater. Res.* **2004**, *19*, 1924–1945.
(52) Thompson, B. C.; Frechet, J. M. J. *Angew. Chem., Int. Ed.* **2006**, *47*, 58–77.
(53) Jo, J.; Kim, S.-S.; Na, S.-I.; Yu, B.-K.; Kim, D.-Y. *Adv. Funct. Mater.* **2009**, *19*, 866–874.
(54) Erb, T.; Zhokhavets, U.; Gobsch, G.; Raleva, S.; Schilinsky, P.; Waldauf, C.; Brabec, C. J. *Adv. Funct. Mater.* **2005**, *15*, 1193–1196.
(55) Yang, X.; Loos, J.; Veenstra, S. C.; Verhees, W. J. H.; Wienk, M. M.; Kroon, J. M.; Michels, M. A.; Janssen, R. A. J. *Nano Lett.* **2005**, *5*, 579–583.
(56) Chikamatsu, M.; Nagamatsu, S.; Yoshida, Y.; Satio, K.; Yase, K. *Appl. Phys. Lett.* **2005**, *87*, 203504/1–203504/3.

AM9006897